Supporting Information for

Designed Formulation of Se-Impregnated N-Containing Hollow Core Mesoporous Shell Carbon Spheres: Multifunctional Potential Cathode for Li-Se and Na-Se Batteries

*Balakumar Kalimuthu and Kalaiselvi Nallathamby**

Electrochemical Power Systems Division, CSIR- Central Electrochemical Research Institute, Karaikudi-630 003, India

Academy of Scientific and Innovative Research, Chennai-600 113, India

Corresponding Author

* E-mail: kalaiselvicecri@gmail.com

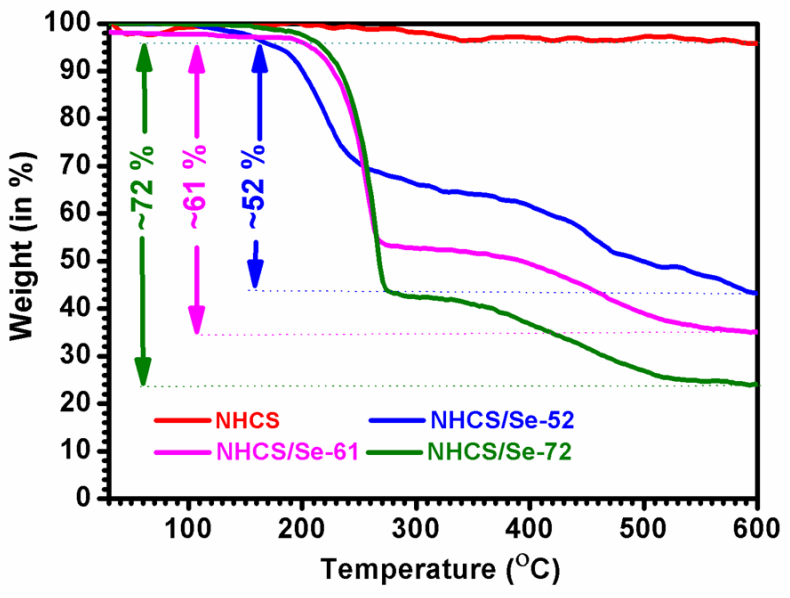

Figure S1. Thermogravimetry analysis of NHCS and NHCS/Se-X (X=52, 61 and 72) composites indicating the presence of confined selenium to the mentioned extent.

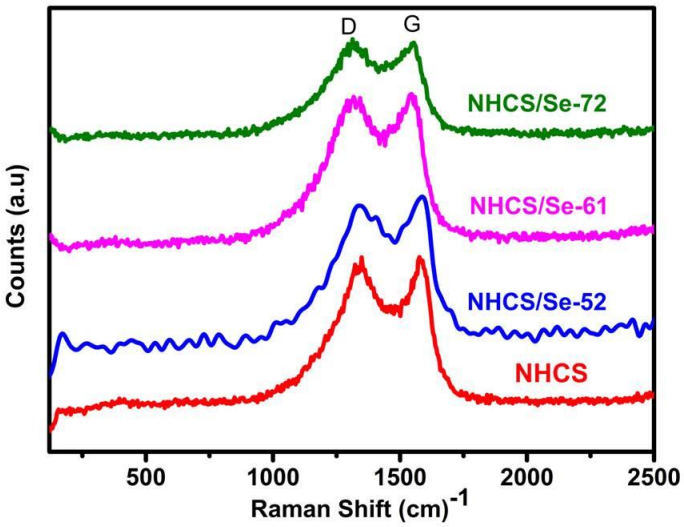

Figure S2. Raman spectrum of NHCS and NHCS/Se-X (X=52, 61 and 72) composites evidencing the better confinement of Se in the pores of NHCS, as no Se peak is found with the composites.

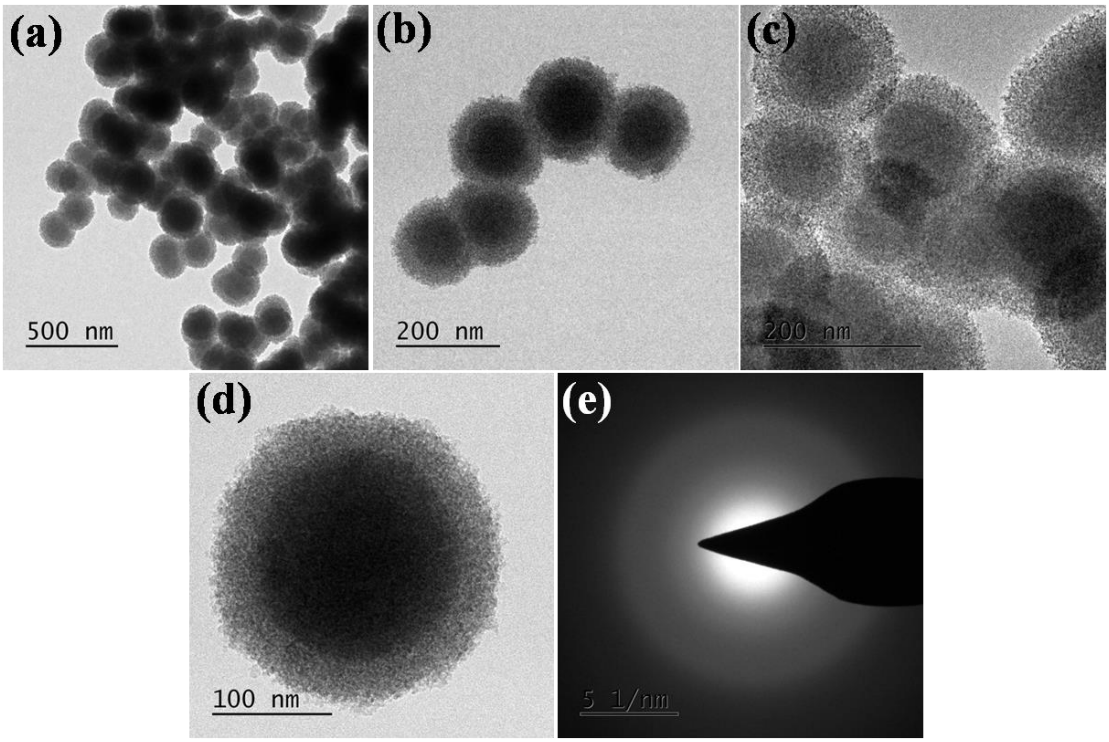

Figure S3. (a)-(e) HRTEM images of solid core and porous shell containing silica beads under different magnifications .

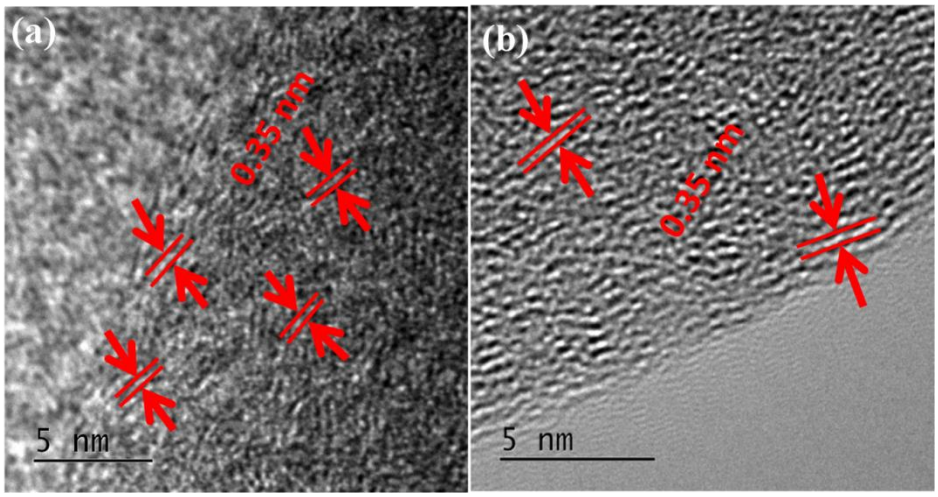

Figure S4. HRTEM image of (a) NHCS and (b) NHCS/Se-52 composite, showing the presence of abundantly available pores that offer scope for easy percolation of electrolyte and facile ion transport kinetics.

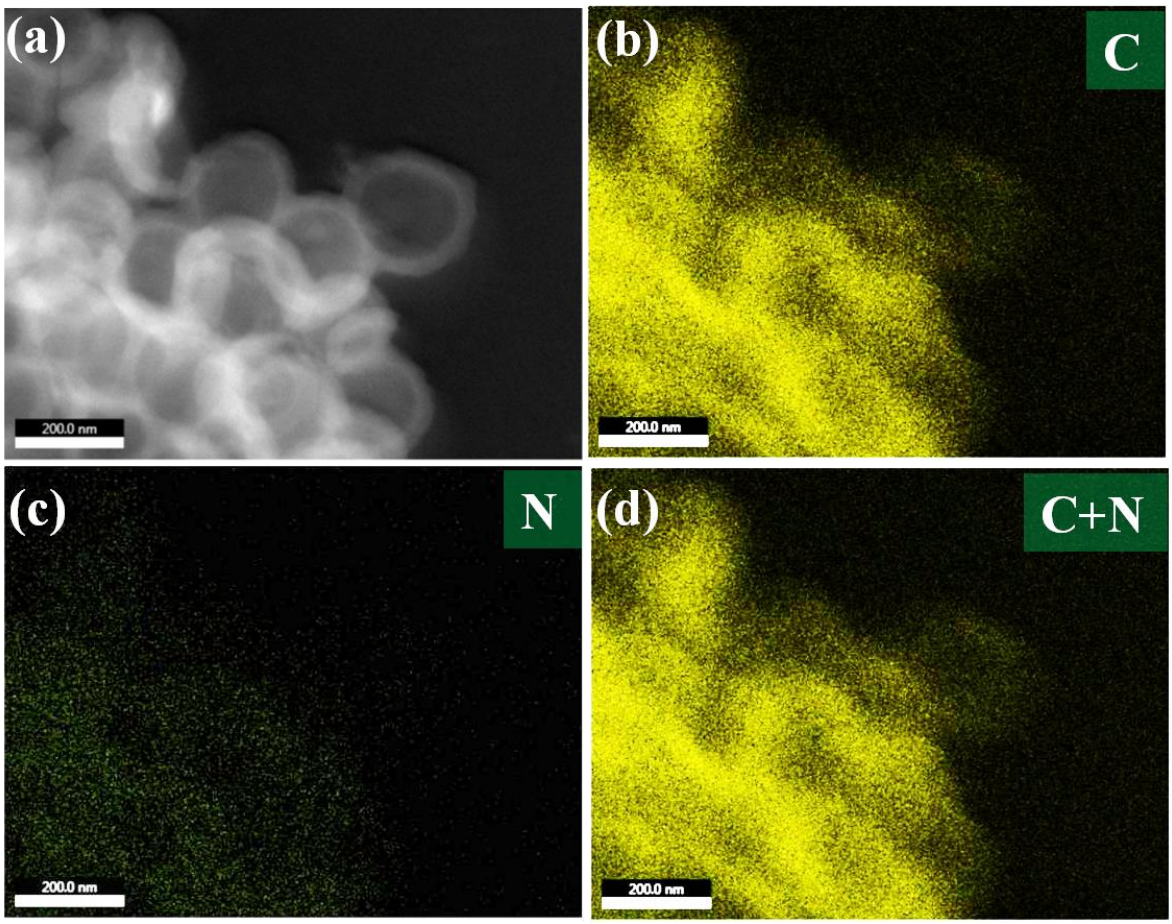

Figure S5. (a) STEM image and (b-d) carbon, nitrogen and cumulative elemental mapping of NHCS, evidencing the uniform distribution of nitrogen in the carbon shell.

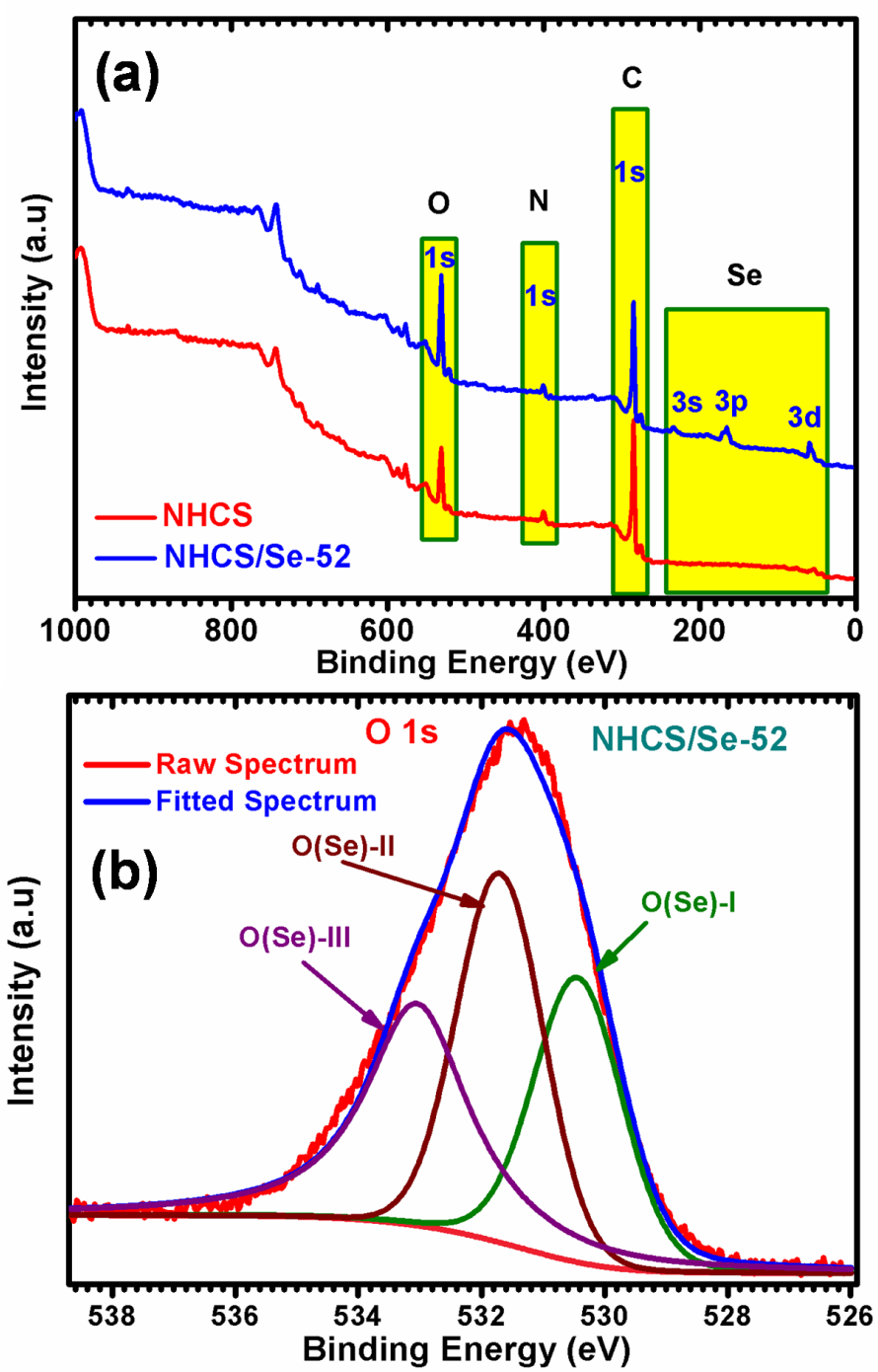

Figure S6. (a) XPS survey spectrum of NHCS and NHCS/Se-52 composite and (b) deconvoluted oxygen 1s photoelectron line of NHCS/Se-52 composite.

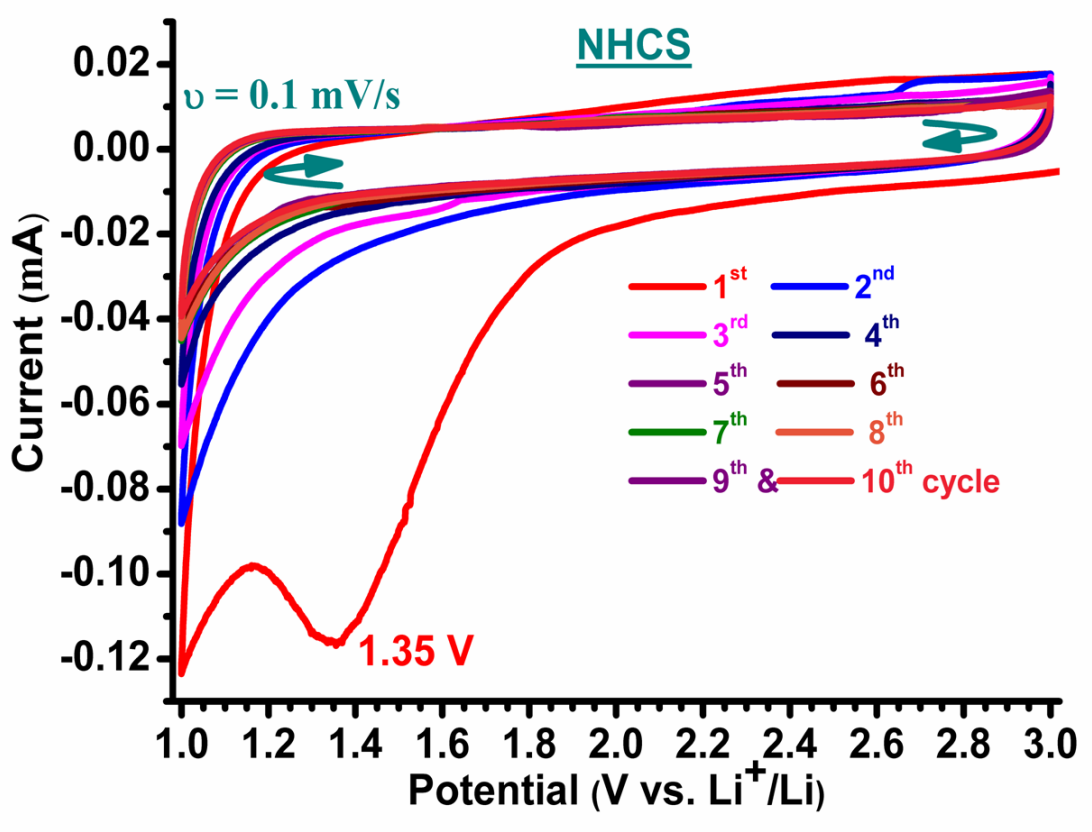

Figure S7. CV behaviour of bare NHCS cathode in the potential window of 1.0 to 3.0 V.

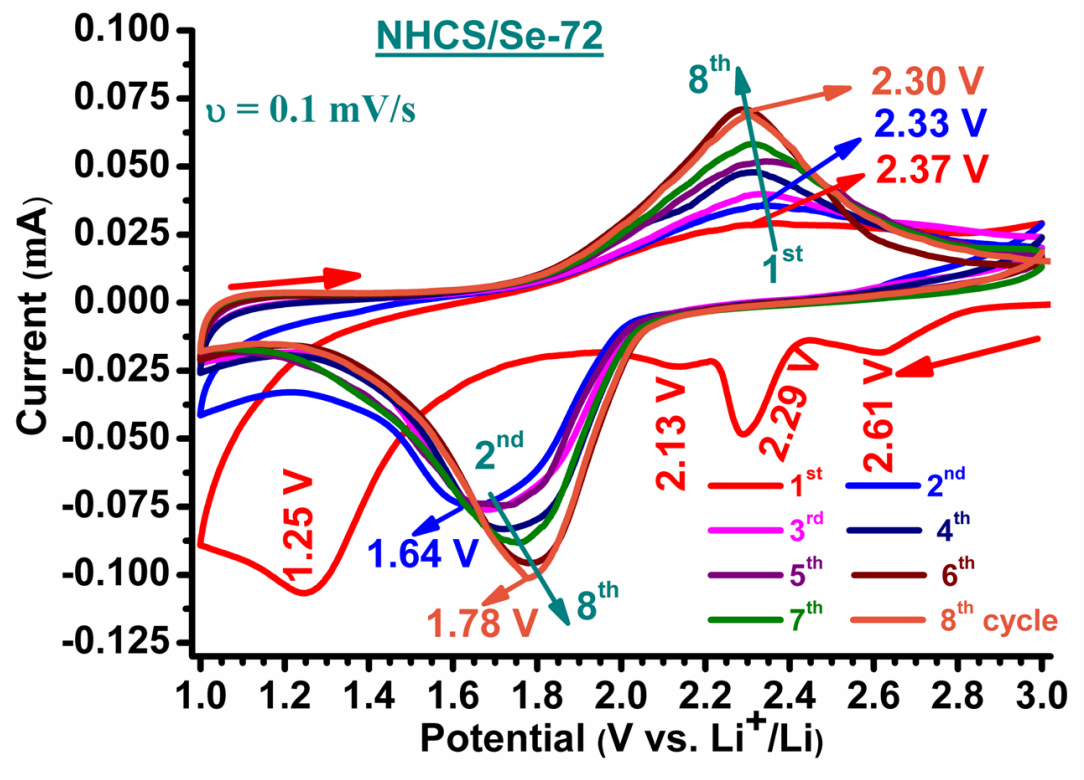

Figure S8. Cyclic voltammogram of NHCS/Se-72 cathode under 0.1 mV/s sweep rate.

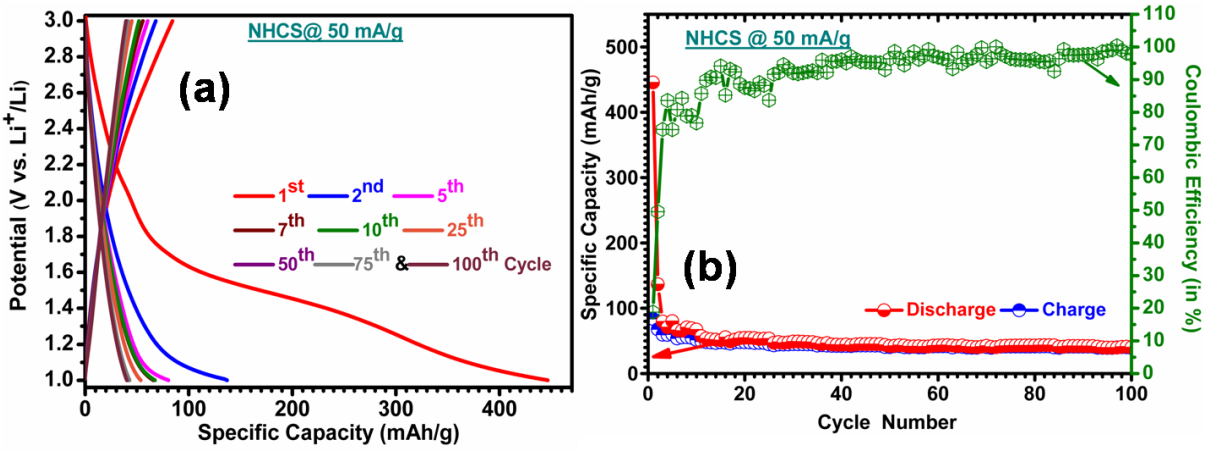

Figure S9. Electrochemical performance of nitrogen doped hollow core mesoshell carbon spheres (NHCS) at 50 mA/g. (a) select cycle voltage profiles and (b) cycleability of NHCS up to 100 cycles.

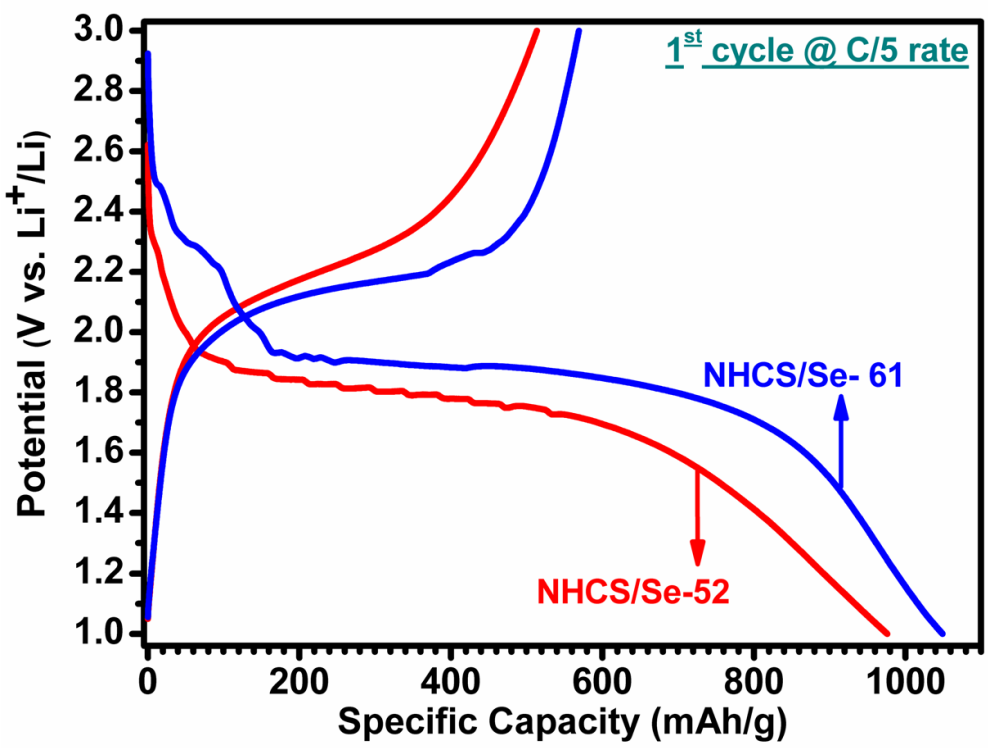

Figure S10. First cycle voltage profile of NHCS/Se-52 & 61 cathode under C/5 rate consisting of initial irreversible discharge plateau in the 2.35-2.20 V region along with the major reduction plateau at ~ 1.8 V, corresponding to the formation of Li_2Se.

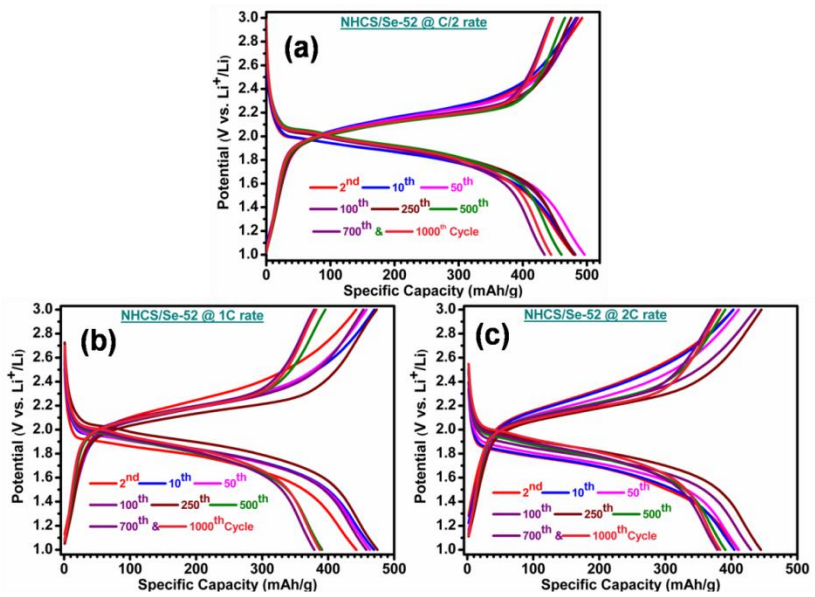

Figure S11. Select cycle voltage profiles of NHCS/Se-52 cathode at (a) C/2, (b) 1C, and (c) 2C rate, revealing perfect overlapping of charge/discharge curves up to 1000 cycles, especially under C/2 rate.

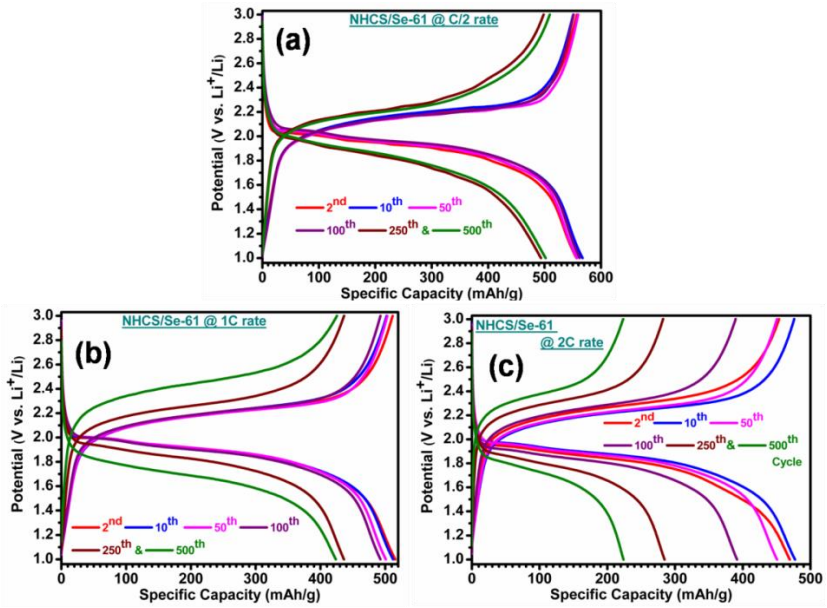

Figure S12 Select cycle voltage profiles of NHCS/Se-61 cathode at (a) C/2, (b) 1C, and (c) 2C rate, wherein increasing polarisation behaviour after 100 cycles is observed at all rates.

Cycleability and rate capability of NHCS/Se-72 cathode

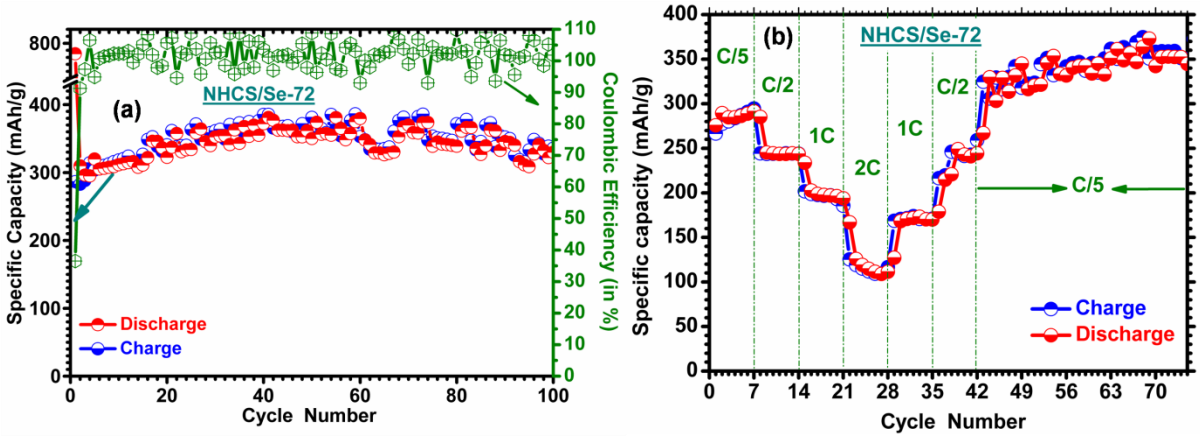

Figure S13. Electrochemical performance of 72 wt.% Se loaded NHCS. (a) Cycleability under C/5 rate and (b) rate capability behaviour, from which capability of NHCS to accommodate 72 wt.% Se loading and to act as a cathode could be understood, irrespective of the inferior capacity values compared with those of 52 and 61 wt.% Se loading.

Cycleability study of 72 wt.% Se loaded NHCS cathode under C/5 rate (Figure S13(a)) shows 310 mAh/g as initial (2^{nd}) capacity, which increases to 350 mAh/g at the 50^{th} cycle and retains about 329 mAh/g at the 100^{th} cycle. This observation in turn helps to understand the fact that NHCS can hold a Se content as high as 72 wt.% and exhibits moderate performance with good reversibility up to a minimum of 100 cycles under C/5 rate. Rate capability study of NHCS/Se-72 cathode (Figure S13(b)) shows moderate capacity values of 290, 240, 198 and 117 mAh/g under C/5, C/2, 1C and 2C rate respectively and the initial capacity of ~ 300 mAh/g has been resumed, when the cell is switched back to C/5 rate. Interestingly, the extended capacity at C/5 rate is found to increase with the increasing cycle number, which is not unusual.

Storage mechanism

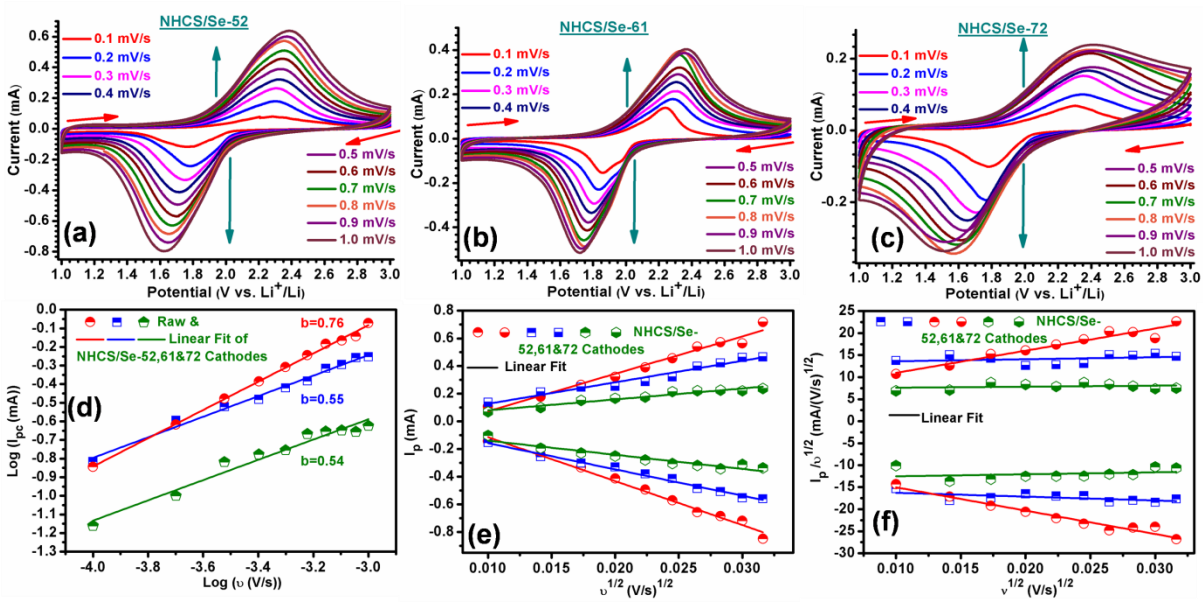

Figure S14. (a)-(c) CV recorded for NHCS/Se-52, 61 & 72 cathodes under different scan rates, (d) power law relationship between peak current and scan rate, (e) peak current vs. square root of scan rate and (f) (square root of) scan rate normalized peak current dependent square root of scan rate plot of NHCS/Se-52, 61 & 72 cathodes.

The outperforming electrochemical behaviour of NHCS/Se-52 cathode with those of NHCS/Se-61 and 72 cathodes could be understood as a function of unfilled pores or void volume towards capacity. In this connection, CV behaviour of NHCS/Se-52, 61 and 72 cathodes at different scan rates has been recorded individually (Figure S14(a-c)) and the relationship between peak current and scan rate has been studied in detail. By using power law (Equation 1), Randles-Sevcik equation (Equation 2) and Equation 3 and 4, comparison of performance of select cathodes (Figure S14(d-f)) has been made.[1, 2] From Figure S14(a-c), variation of scan rate as a function of peak current is found to be in order, which is the characteristic behaviour of perfectly reversible electrodes. Notably, NHCS/Se-61 and 72 cathodes exhibit diffusion controlled mechanism associated with the process of charge/discharge, whereas NHCS/Se-52

cathode represents a combination of diffusion controlled as well as surface storage mechanism due to the effect of unfilled pores. Such a combination is believed to be helpful in endorsing NHCS/Se-52 cathode for its suitability at high rates along with extended cycle life, as discussed under charge/discharge studies. Hence, the requirement of sufficient void volume to buffer the volume expansion of electrode upon cycling, apart from the basic requirement of confinement and effective utilization of Se could be understood. From Figure S14, one can understand that NHCS/Se-52 cathode, bestowed with all the said desired properties enjoy the synergistic advantages to qualify itself for extended cycles and high rate application in Li-Se system.

$I = a\nu^b$ --- (1)

Where I -current (A), ν-scan rate (V/s), a and b- adjustable parameters

$I_p = (2.69 \times 10^5) n^{3/2} A D_o^{1/2} C_o^* \nu^{1/2}$ ---(2)

Where, I_p- peak current (A), n- number of electron transferred, A- electrode area (cm^2), D_o- diffusion coefficient (cm^2/s), C_o^* -reactant concentration (mol/cm^3) and ν- scan rate (V/s).

$I_{pc}(V) = k_1\nu + k_2\nu^{1/2}$ --- (3)

where, $k_1\nu$ and $k_2\nu^{1/2}$ -current due to capacitive and diffusion controlled insertion process and rearranged as

$\frac{I_{pc}(V)}{\nu^{1/2}} = k_1\nu^{1/2} + k_2$ --- (4)

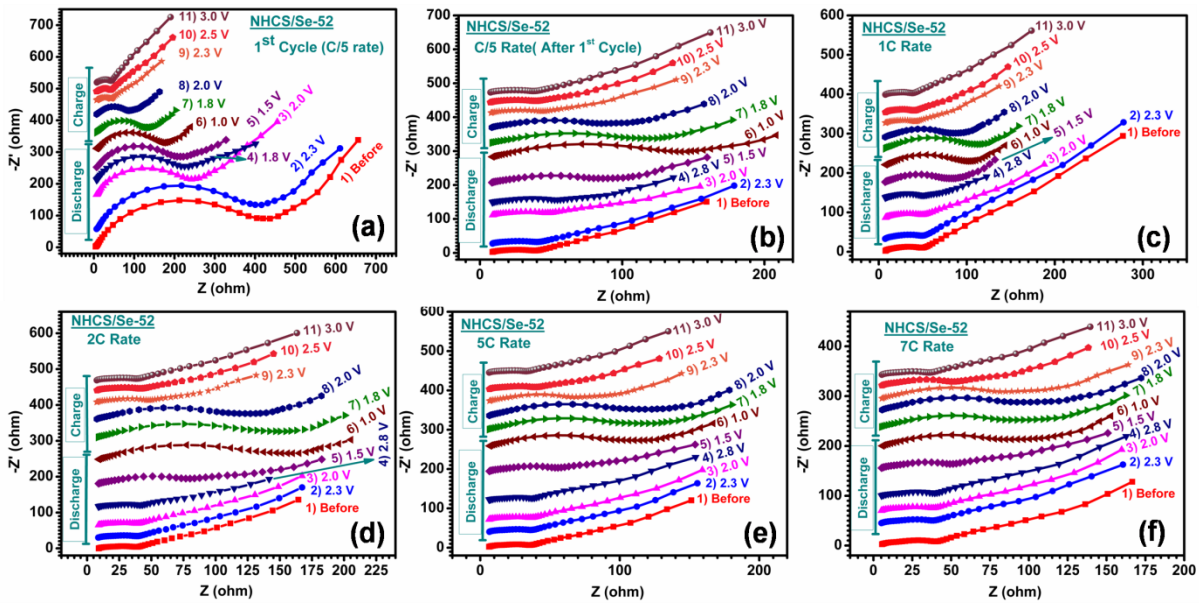

Figure S15. Nyquist plot of NHCS/Se-52 cathode as a function of depth of discharge (DOD) and depth of charge (DOC) at various rates. Electrochemical impedance spectrum recorded during (a) first and (b) after first cycle at C/5 rate, (c) 1C, (d) 2C, (e) 5C and (f) 7C rate.

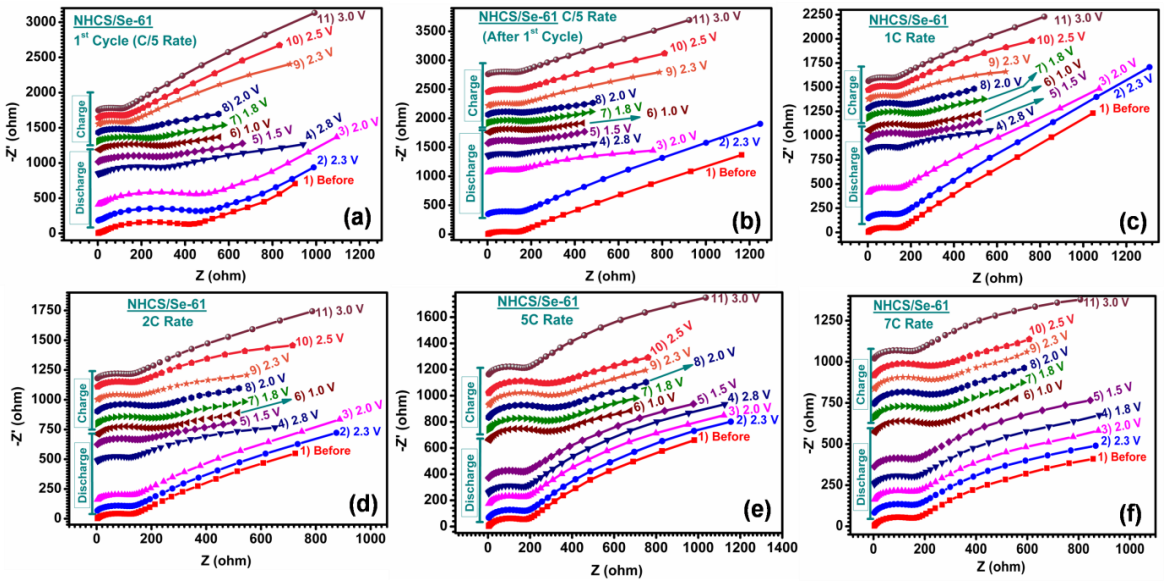

Figure S16. Nyquist plot of NHCS/Se-61 cathode as a function of DOD and DOC at various rates. Electrochemical impedance spectrum recorded during (a) first and (b) after first cycle at C/5 rate, (c) 1C, (d) 2C, (e) 5C and (f) 7C rate showing the attainment of original value at the end of charge.

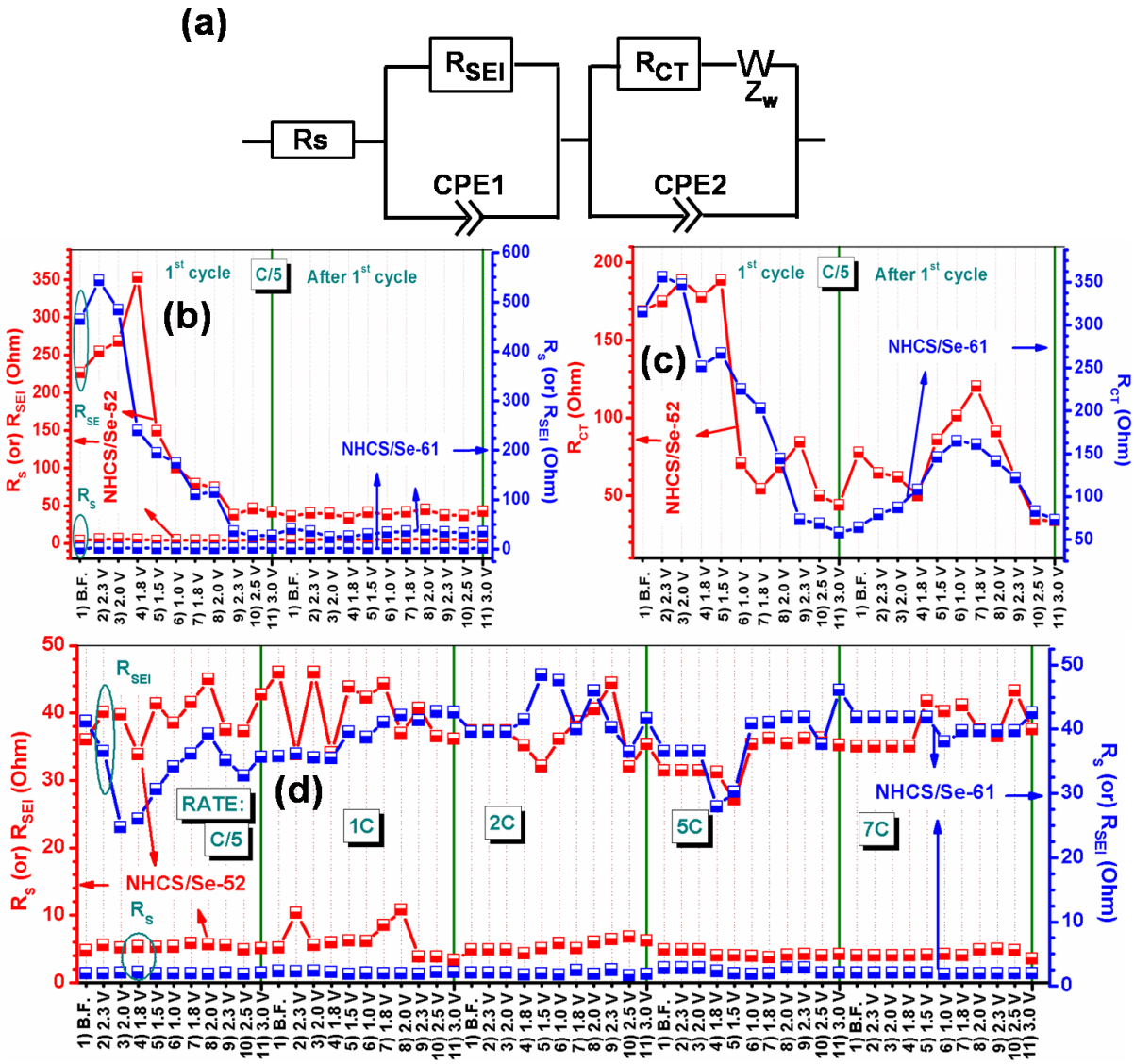

Figure S17. (a) Equivalent circuit model used to fit the Nyquist plot of NHCS/se-52 and 61 cathode containing cells. Plots (b-d) consist of fitted parameters as function of DOD and DOC for different cycle number/C-rates. (b) Solution (or electrolyte) resistance (R_S) and resistance due to SEI (R_{SEI}) and (c) charge transfer resistance (R_{CT}) during first and after first cycle tested at C/5 rate and (d) R_s and R_{SEI} values under different C-rates for NHCS/se-52 and 61 cathode containing cells.

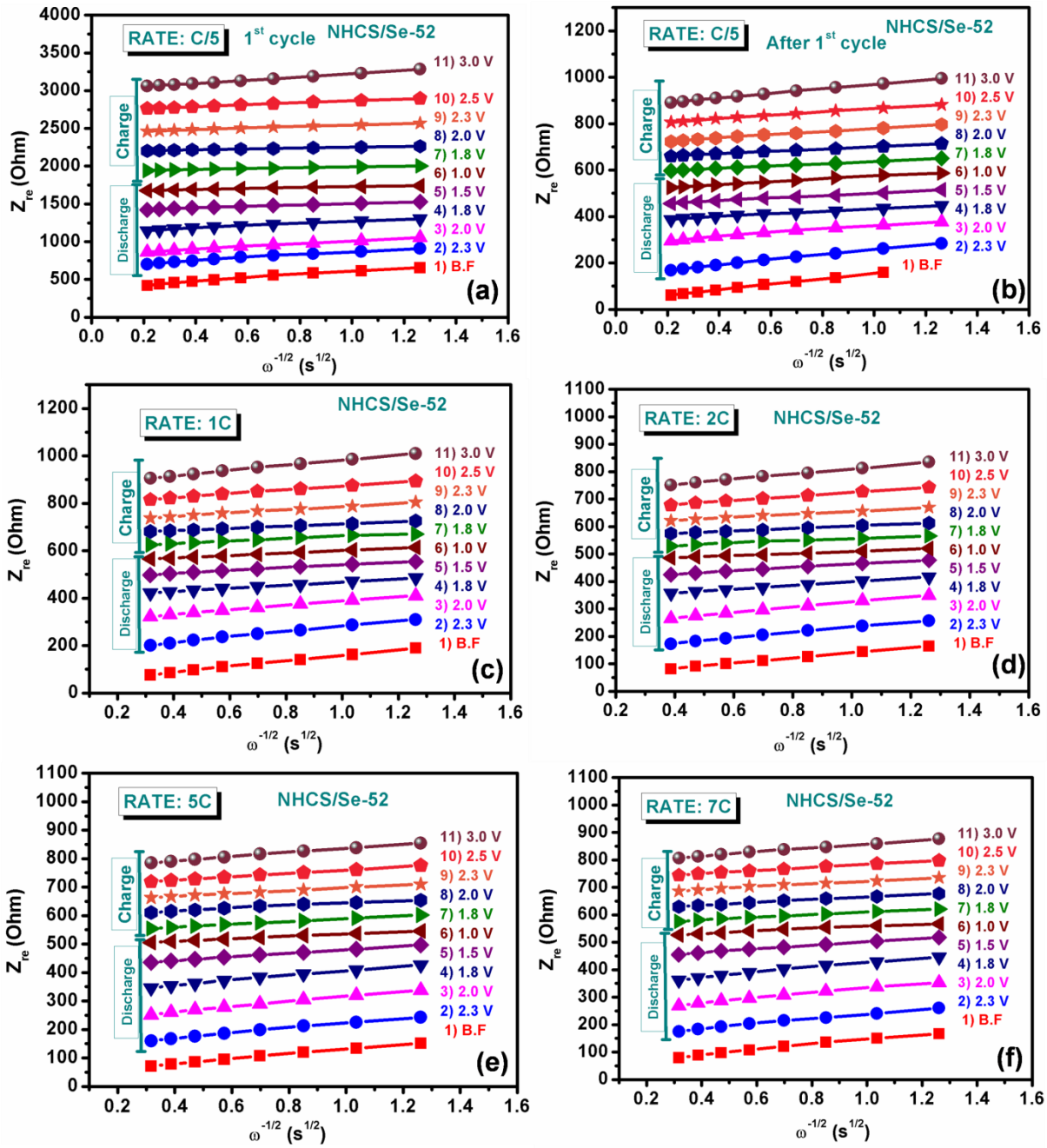

Figure S18. (a-f) Z_{re} – $\omega^{-1/2}$ plot of NHCS/Se-52 cathode containing cell as a function of DOD and DOC under the influence of different C-rates to deduce the Warburg factor σ_w.

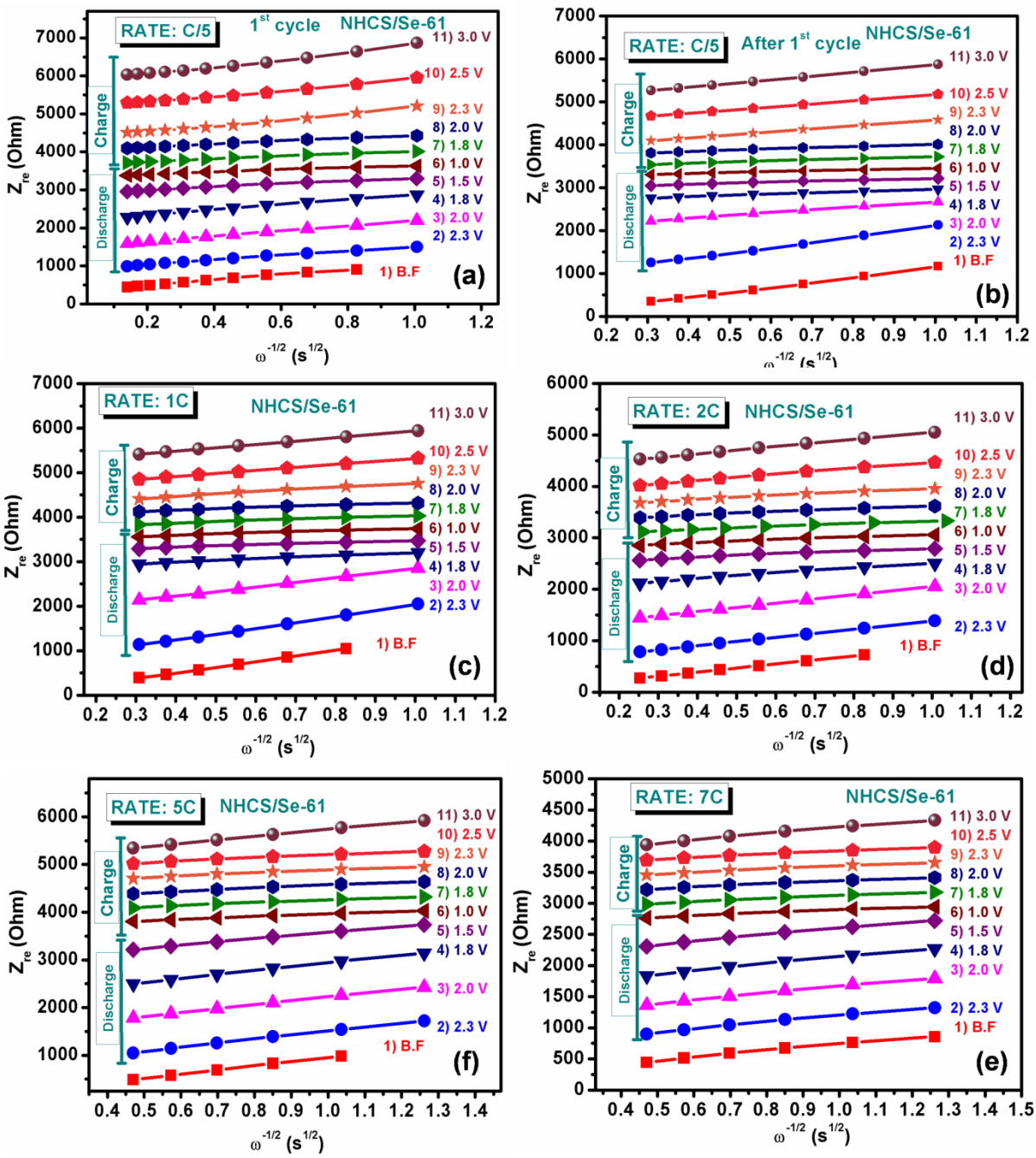

Figure S19. (a-f) $Z_{re} - \omega^{-1/2}$ plot of NHCS/Se-61 cathode containing cell as function of DOD and DOC under the influence of different C-rates used to deduce σ_w.

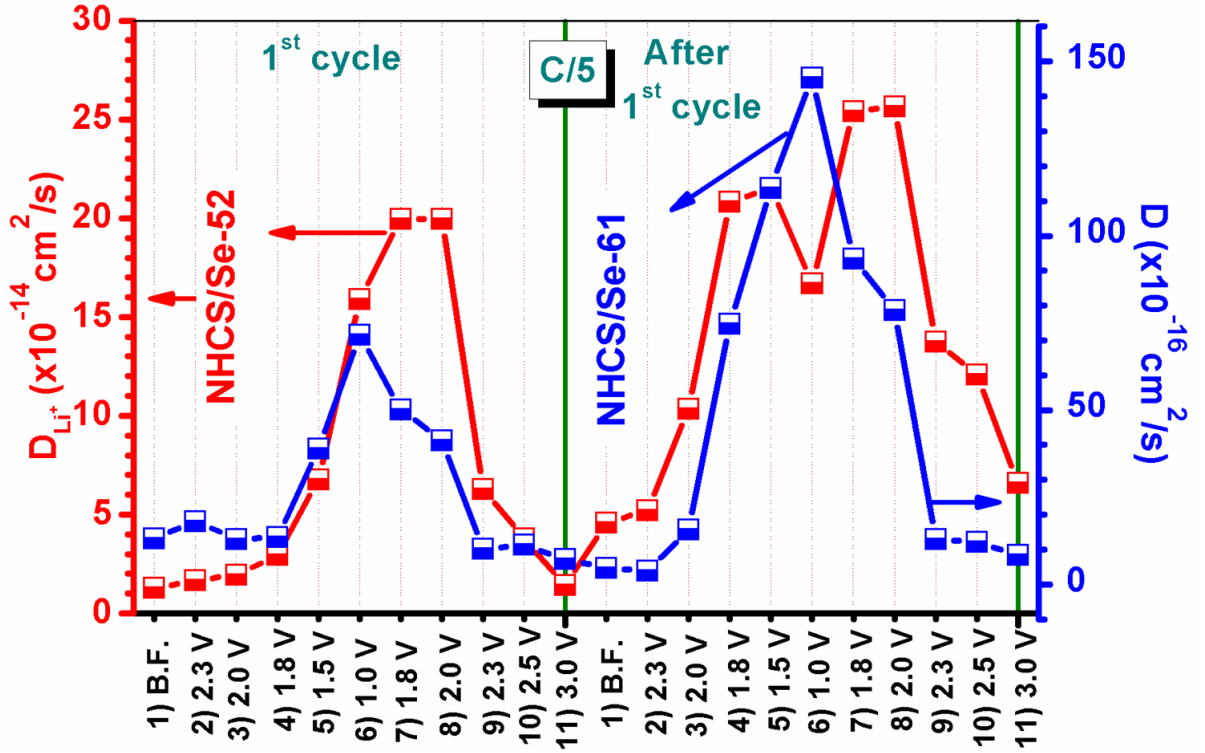

Figure S20. Li-ion diffusion co-efficient of NHCS/Se-52 and 61 cathode containing cells as function of DOD and DOC during first and after the first cycle (C/5 rate).

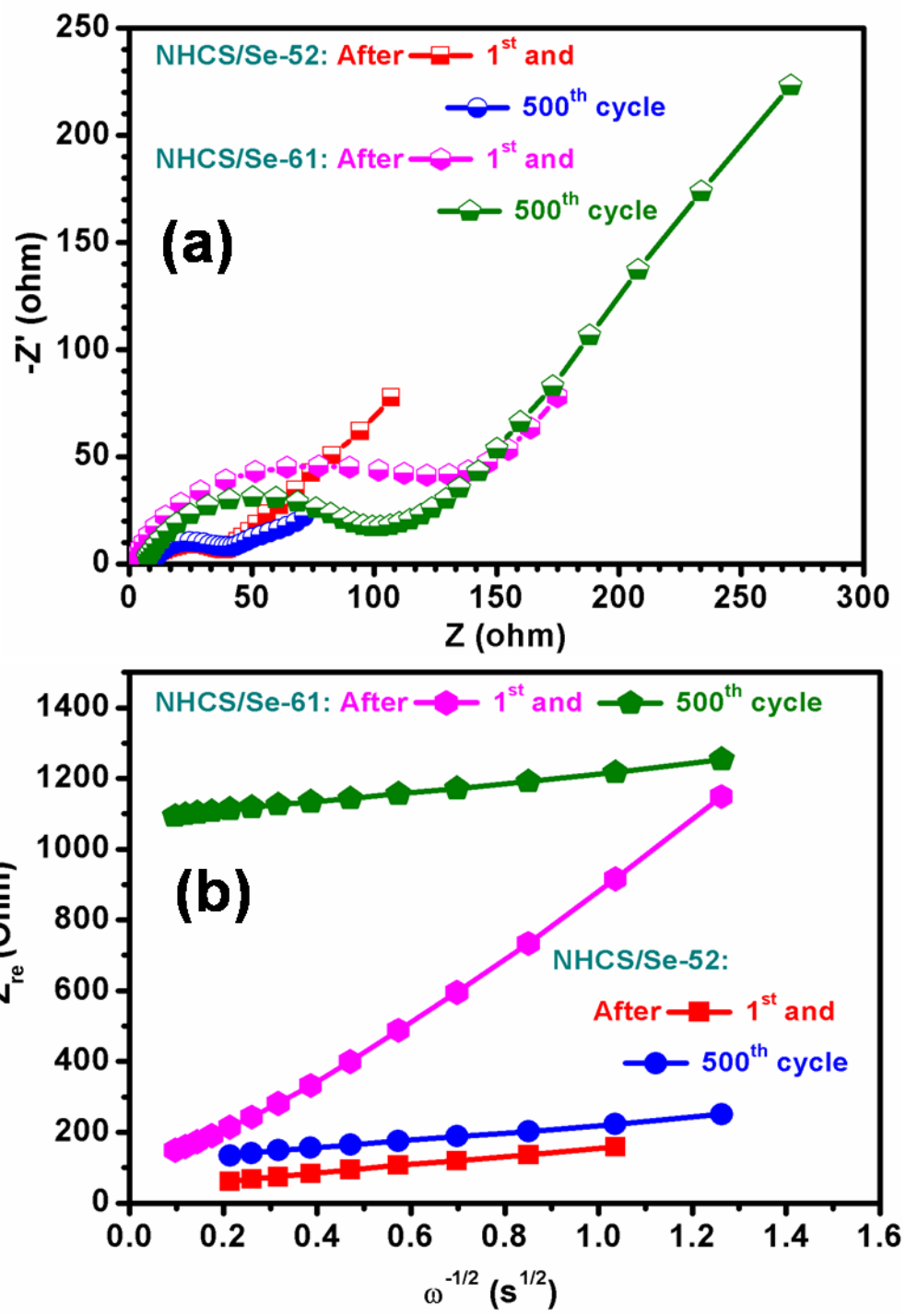

Figure S21. Comparative (a) Nyquist plot and (b) Z_{re} - $\omega^{-1/2}$ plot of NHCS/Se-52 and 61 cathode containing cells at different cycling conditions, revealing the constant lithium diffusion coefficient and the substantially increased D_{Li^+} of NHCS/Se-52 and 61 cathodes.

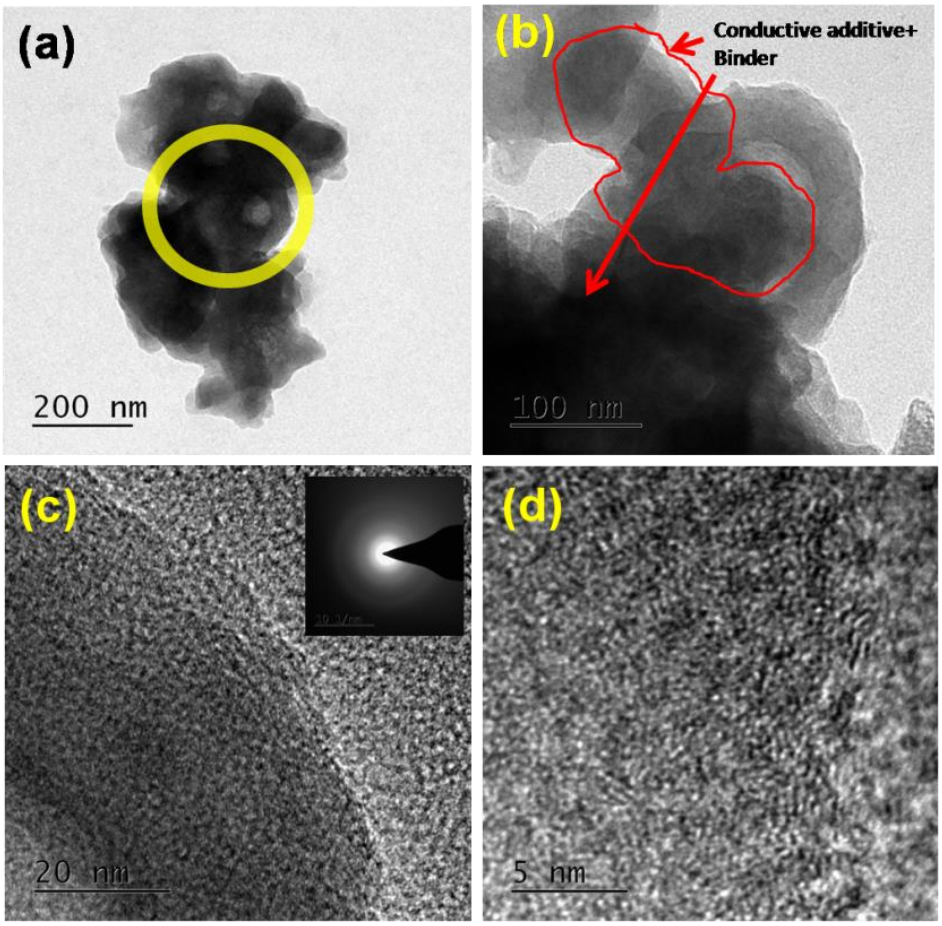

Figure S22. (a-d) HRTEM images of NHCS/Se-52 cathode after 500 cycles at 2C rate. Inset of (c): SAED pattern.

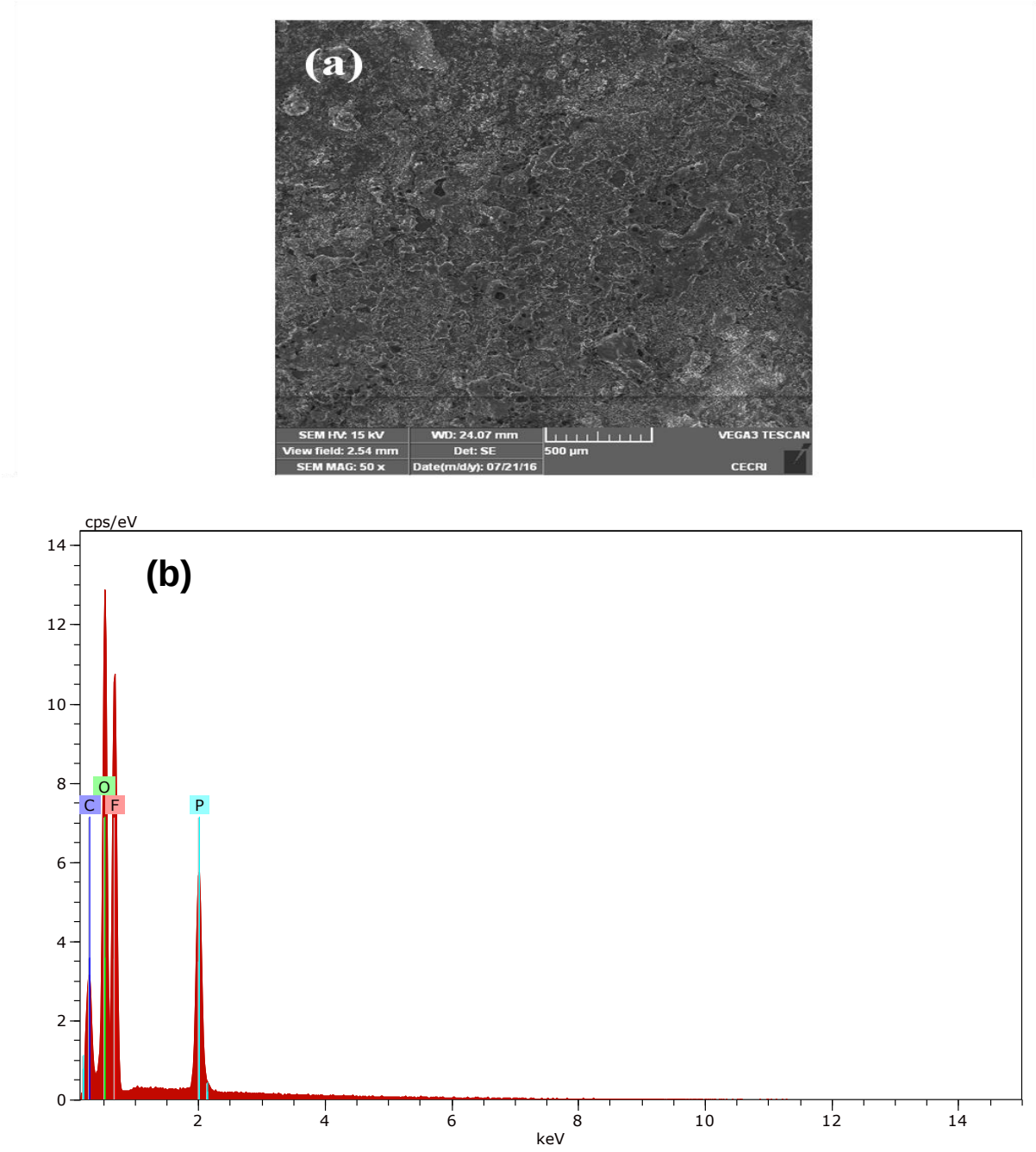

Figure S23. Post cycling (a) SEM image and (b) EDX spectrum of Li surface, indicating the absence of Se and ensuring the absence of undesired redox shuttle reactions.

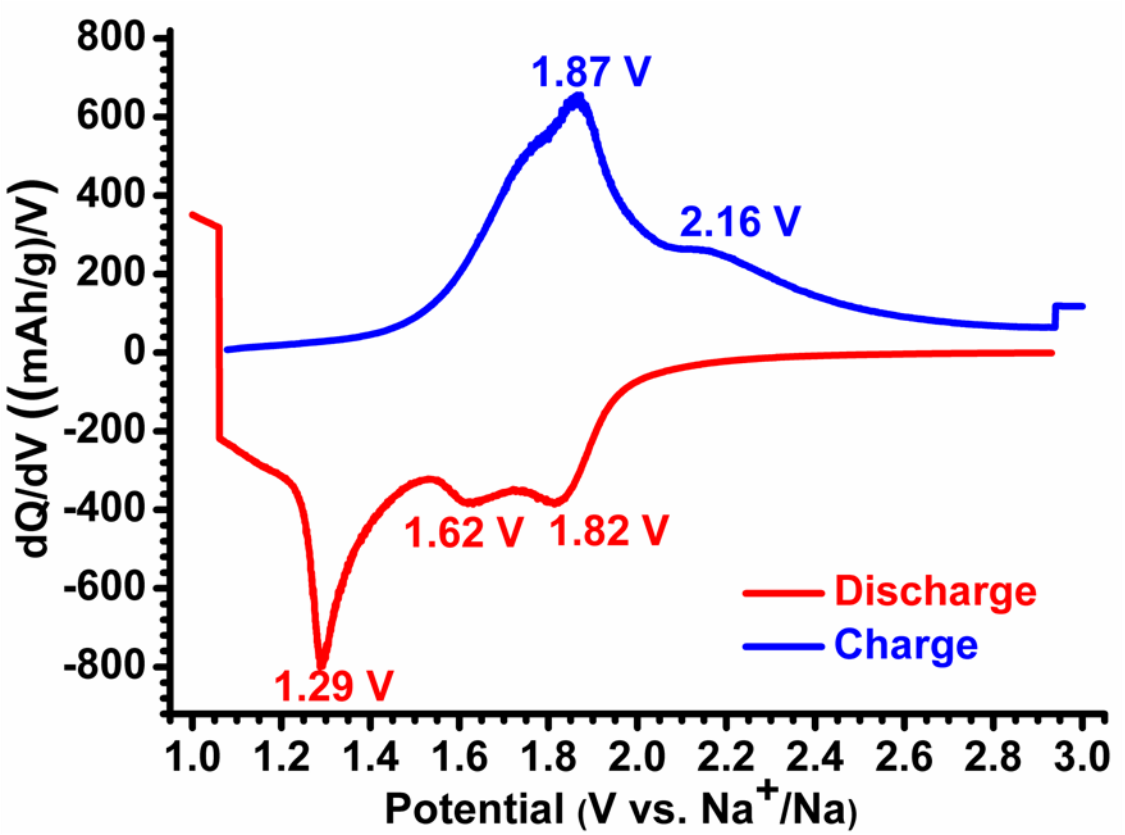

Figure S24. dQ/dV vs. potential plot of NHCS/Se-52 cathode under C/5 rate observed in Na-Se assembly.

REFERENCES

(1) Wang, J.; Polleux, J.; Lim J.; Dunn, B. Pseudocapacitive Contributions to Electrochemical Energy Storage in TiO_2 (Anatase) Nanoparticles. *J. Phys. Chem. C* **2007**, *111*, 14925-14931.

(2) Liu, S.; Hui, K. S.; Hui, K. N.; Yund, J. M.; Kim, K.H. Vertically Stacked Bilayer $CuCo_2O_4/MnCo_2O_4$ Heterostructures on Functionalized Graphite Paper for High-Performance Electrochemical Capacitors. *J. Mater. Chem. A* **2016**, *4*, 8061-8071.